ELSEVIER

Journal of Hazardous Materials 49 (1996) 247–265

JOURNAL OF HAZARDOUS MATERIALS

Vacuum extraction of a nonaqueous phase residual in a heterogeneous vadose zone

J.L. Smith [a], D.D. Reible [a,*], Y.S. Koo [b], E.P.S. Cheah [b]

[a] *Department of Chemical Engineering, Louisiana State University, Baton Rouge, LA 70803, USA*
[b] *Department of Chemical Engineering, The University of Sydney, Sydney, NSW 2006, Australia*

Received 1 April 1995; accepted 5 February 1996

Abstract

The fate of an infiltrating nonaqueous phase liquid (NAPL) in a heterogeneous vadose zone was evaluated under laboratory conditions. Vapor extraction was then used to remove the contaminant, and the rate of removal was compared with the predictions of simple mathematical models. The laboratory experiments were conducted in idealized soil systems in which a fine-grained, low permeability lens insert was located in a coarse-grained sand layer.

The infiltration study indicated that an essentially saturated layer of NAPL was trapped at the *base* of a fine-grained lens. A model of this process showed that capillary forces were responsible for the observed retention. Entrapment of NAPL within the fine-grained lens was expected to reduce the effectiveness of any in-situ extractive technology such as soil vacuum extraction (SVE) for the removal of the NAPL. Simple models of the mass transfer from the lens-entrapped NAPL to an extracting vapor in the coarse sand layer were developed and applied to laboratory experiments in which toluene, either pure or in a mixture, was injected within an idealized low permeability lens. Mass transfer resistances in the extracting vapor-phase controlled the release of pure toluene from the fine lens at low air flowrate (Reynolds number, $Re \leq 0.5$) while intra-lens diffusion resistances were dominant at higher air flow rate ($Re \geq 3$). Liquid phase resistances were always important in the extraction of toluene from a NAPL mixture. The models were found to accurately predict the removal rate of the toluene from the low permeability lens under each of the experimental conditions.

Keywords: Heterogeneous vadose zone; Nonaqueous phase liquid; Vacuum extraction

* Corresponding author. Tel: 504-388-6770; Fax: 504-388-5043.

PII S0304-3894(96)01761-X

1. Introduction

A variety of technologies have been developed to remediate contaminated soils. The soil vacuum extraction (SVE) process has gained popularity in recent years to remove volatile contaminants such as chlorinated solvents and volatile gasoline components in the unsaturated zone. In the SVE process, a subsurface pressure gradient generated by a vacuum pump induces air flow through the contaminated soil. The passing air incorporates the volatile contaminants in the soil and transports them to a recovery well. Contaminant-laden air exiting the recovery well is then either vented to the atmosphere or treated, depending upon the contaminant concentration in the exiting air. Surface operations during SVE are simple and the required equipment is relatively inexpensive. It is also effective for the removal of the most volatile contaminants which often constitute the greatest hazards to groundwater. A number of reported pilot and field scale applications of the process have shown its effectiveness in cleaning up contaminated soils [1,2].

Although SVE has been shown to be effective in reducing contaminant levels in soils, there are limitations to its use. For example, it has been acknowledged that the process is generally not feasible or must be modified when most of the soil contaminant lies on or below the water table. Nor is it feasible in relatively low permeability soils or when the compounds to be removed are of low volatility. Other problems in the SVE process are air short-circuiting, reducing the efficiency of the remediation [3], and groundwater upwelling in the vicinity of the vacuum well, which may result in the contamination of clean groundwater. Short-circuiting, or flow by-passing is often encountered in any in-situ extractive process for soil remediation. Because of the low viscosity (and therefore low pumping costs) and the large equilibrium capacity of air for many volatile organics, however, these problems are likely to be less severe for SVE than for other fluid extraction technologies such as groundwater pump and treat.

Recent field studies [3–7] and large scale model studies [8,9] have demonstrated the effectiveness of the SVE process. Laboratory scale experiments have also been conducted in one-dimensional and homogeneous sand columns under equilibrium [10,11] and non-equilibrium [12] effluent conditions. Although these laboratory experiments provided insight into the mechanism of contaminant transport, extrapolation of their results to more realistic soil systems, i.e., three-dimensional and heterogeneous soils, is questionable. There is little experimental data in heterogeneous soils except in the field where it is difficult to isolate individual processes. There exist simple models of SVE of volatile contaminants from low permeability lenses [13,14] but these remain largely invalidated either in the field or in the laboratory.

A series of laboratory experiments in idealized heterogeneous soils was conducted to help understand the transport and fate of a spilled oily phase or nonaqueous phase liquid (NAPL) and the removal of its volatile components via SVE. The objective of the work was to determine the ultimate residual distribution of a spilled NAPL in the heterogeneous soil system, and the development and testing of simple mathematical models predicting the rate of NAPL evaporation and removal from the contaminated soil systems.

2. Experimental setup

Two sets of experiments in heterogeneous soils were performed; one focused on the infiltration of the spilled NAPL and resulting distribution of the residual NAPL, and the other focused on removing the volatile components of the NAPL residual via SVE.

2.1. NAPL infiltration

The first set of experiments was conducted by spilling a finite volume (500 mL) of nonvolatile NAPL on the surface of coarse sand confined to a Lexan® tank 104 cm × 104 cm × 5.1 cm width. A fine-grained, low permeability sand "lens" was located within the upper coarse sand layer. A vacuum well was placed near the center of the tank but was unused in this series of experiments. The primary objective of these experiments was to identify the volume the form of NAPL retained by the fine-grained lens. A schematic of the experimental setup for NAPL infiltration is shown in Fig. 1. Physical properties of the fine and coarse sands are listed in Table 1. Sand designated number 363 was used to form the fine sand lens and number 375 was used for the coarse sand layers. The permeabilities in the two sands differed by approximately an order of magnitude. After packing the coarse sand and forming the heterogeneous lens in this layer, gamma-ray attenuation was used to check the uniform packing of the sands. The details of sand placement and the gamma-ray attenuation procedures can be found in Smith [2].

Before initiation of an experiment, typical field moisture conditions were obtained by saturating the sand with water, and then dropping the water level and allowing the sand to drain. This procedure produced a residually water-wetted vadose zone, a saturated region defined by a water table near the bottom of the tank, and a tension saturated

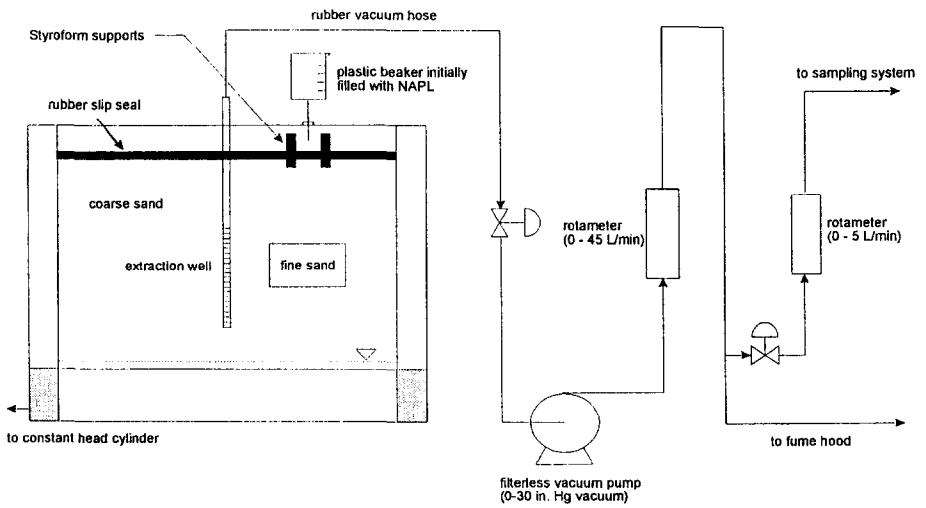

Fig. 1. Experimental apparatus for NAPL infiltration and SVE experiments (not to scale).

Table 1
Physical and hydraulic characteristics of the experimental sands

Sand no.	363	375
Average hydraulic conductivity ($cm\,s^{-1}$)	0.102	1.09
Moisture content (%)	10.0	9.0
Porosity	0.42	0.37
Capillary fringe height (cm)	28.0	6.0
Average particle diameter (mm)	0.21	1.10
Bulk density ($g\,cm^{-3}$)	1.74	1.64

region (or capillary fringe) on top of the water table. Gamma-ray attenuation was also used to quantify the water saturation distribution within the soil. Toluene or automatic transmission fluid (ATF) was used as a NAPL in the infiltration experiments. The NAPL was released into a "well" created by Styrofoam® supports to contain the liquid on the top of the sand. The movement of the oily phase with time was then observed and photographed for further analysis.

2.2. *Vacuum extraction experiments*

These experiments were conducted to quantify the rate of mass transfer from the residual NAPL trapped within the low-permeability lens to the vapor extracting phase. The oily phase was injected directly into the lens in these experiments to simulate the essentially saturated pooling observed at the bottom of the lens during the infiltration experiments. Either pure toluene or a mixture of toluene and non-volatile automatic transmission fluid were used as the oily phase. The air flowrate in the vadose zone, i.e., in the coarse sand layer, was varied to explore the importance of the vapor-phase resistances for each experiment.

The experimental setup is also shown in Fig. 1. The techniques used to fill the tank with the experimental sands and to residually wet the sands with water were the same as those used in the oily phase infiltration experiments. The size of the inserted lens was 14 cm in length, 4 cm in height, and 5.1 cm in width. A vacuum extraction well was installed near the center of the tank. The top of the sand and the side of the tank closest to the well were sealed to prevent air short-circuiting and to ensure largely one-dimensional air flows around the lens.

A gas impinger filled with hexane was used to absorb toluene from a side stream taken from the extracted vapors. The sampling time was normally 5 mins and the flowrate of the extracted vapor was measured. The absorbed toluene mass was quantified by gas chromatography with flame ionization detection. The extracting vapor concentration was then calculated by dividing the total mass by measured vapor flowrate and sampling time. The absorption efficiency of the impinger was determined by passing an air stream contaminated with a known concentration of toluene through the impinger. The sampling stream flowrate was set to maximize the adsorption of toluene and to minimize sensitivity to flowrate [2].

2.2.1. Pure toluene

To examine the rate of mass transfer without any mixture related liquid-phase resistances in the lens, pure toluene was first used as the experimental NAPL. Toluene was directly injected into the lens through a 2 mm diameter and 200 mm long tube. The injection was performed slowly to ensure that capillarity was controlling the final distribution of the NAPL as would be the case for slow infiltration by gravity from the surface. After 30 cm^3 of toluene had been injected, the sides of the lens was reached and the injection was halted. The upper 1.4 cm of lens were filled with toluene. To insure containment of the low viscosity toluene in the lens, sufficient volume of NAPL was not introduced to cause displacement of the residual water at the base of the lens. The presence of water-filled pores at the base of the lens suggested that vapor movement would only occur from the upper surface of the lens. To examine the effect of the vapor-phase resistances on the overall mass transfer, a low air velocity in the vadose zone was first maintained during the extraction process. The air flowrate was then increased to minimize the vapor-phase resistance. In the low flowrate stage, the interstitial air velocity (V_x) was 0.73 cm s^{-1} (at atmospheric pressure), corresponding to a Reynolds number (Re) based on the average particle diameter of about 0.5. Under the high air flow conditions, V_x and Re were 4.7 cm s^{-1} and 3.0 respectively.

2.2.2. Oily phase mixture

Finally, to indicate the effect of liquid phase diffusional resistances, an oily phase mixture composed of 5% toluene and 95% ATF was used. The experimental setup for these experiments was essentially the same as the pure toluene experiment. A total of 85 cm^3 of the mixture was injected. The lower viscosity of the oil made it possible to displace the water in the cell without simultaneously depleting the oil. It was expected that both the top and bottom surfaces of the oily phase were exposed to the extractive air phase and available for vapor movement.

3. Results and discussion

3.1. Contaminant infiltration

The most significant result of the infiltration experiments was the retention of a large amount of the residual NAPL at the base of the fine lens in the coarse sand layer. Normally, oily phase contaminants might be expected to pool on the surface of a fine-grained, low permeability region. The ability of the NAPL to displace the non-wetting air phase in the vadose zone, however, suggests that capillary effects can ultimately result in larger NAPL saturations within the lens and not on its surface.

The process of NAPL penetration into the fine lens was expected to be a three step process:

1. Displacement of air from the fine lens allowing infiltration of the NAPL into the lens,
2. Pooling of the NAPL on the surface of the residual water held at high saturations near the bottom of the fine lens,

Table 2
Physical characteristics of sands used in modeling of NAPL infiltration

Sand	Fine	Coarse
Absolute permeability (md)	2000	200
Residual water content (%)	20.0	20.0
Porosity	0.40	0.30

3. Displacement of the mobile water once the pooling is sufficient to overcome the head differential in capillary suction between the fine lens and the underlying coarse material. The water displacement would be expected to continue until the water saturation and associated capillary suction differential between the lens and the underlying material is greater than the driving head of the pooled NAPL.

Thus, the discontinuity in capillary suction between the fine lens and underlying coarse material resulted in the largest NAPL saturations above the *base* of the lens. In the experiment, the NAPL saturation at the base of the lens was about 75% and residual water filled the remainder of the pore space. In contrast to this behavior, a dense NAPL in the saturated zone would be expected to pool on top of a fine grained lens rather than penetrate. Below the water table, the NAPL would generally be unable to displace the more wetting water without the assistance of capillary forces from the soil below the lens.

In order to examine this process more closely, a model of water-oil-air flow in a porous medium was developed. It was assumed that the phases were immiscible and the effect of mass transfer on the phase saturation was expected to be negligible. Simulations were performed using IMEX 300-DX, a black oil reservoir simulator produced by the Computer Modeling Group, Canada [15].

The two-dimensional grid used in the model was largely composed of a coarse sand with a fine grained lens located near the center. The physical properties of the sands are tabulated in Table 2. Capillary pressure and relative permeability functions were modified from Slider [16] and Honarpour *et al.* [17]. Initially, the soil was residually water saturated. In addition, soil near the surface was also saturated with oil which was then allowed to drain by gravity. A constant pressure boundary was imposed at the soil surface. The simulation was allowed to proceed until changes in oil saturation were negligible.

For comparison, the static oil distribution was also calculated. If there was an infinitely large pool of oil at the base of the sand system, some oil will be drawn into the sand above this pool. The resulting non-zero static oil distribution above the pool represents the oily phase saturation which is a result of capillary forces.

Solution of the model resulted in the NAPL distribution shown in Fig. 2. Also shown is the static oil distribution. The model predicted oil distribution agrees qualitatively with experimental observation. This distribution also matches the static distribution, suggesting that the ultimate oil distribution is largely the result of capillary forces. Thus, the presence of the low permeability but high capillarity lens results in entrapment of an essentially saturated zone of NAPL. Simulations with different permeability and capillarity contrasts including clay type lenses in the unsaturated zone showed similar results.

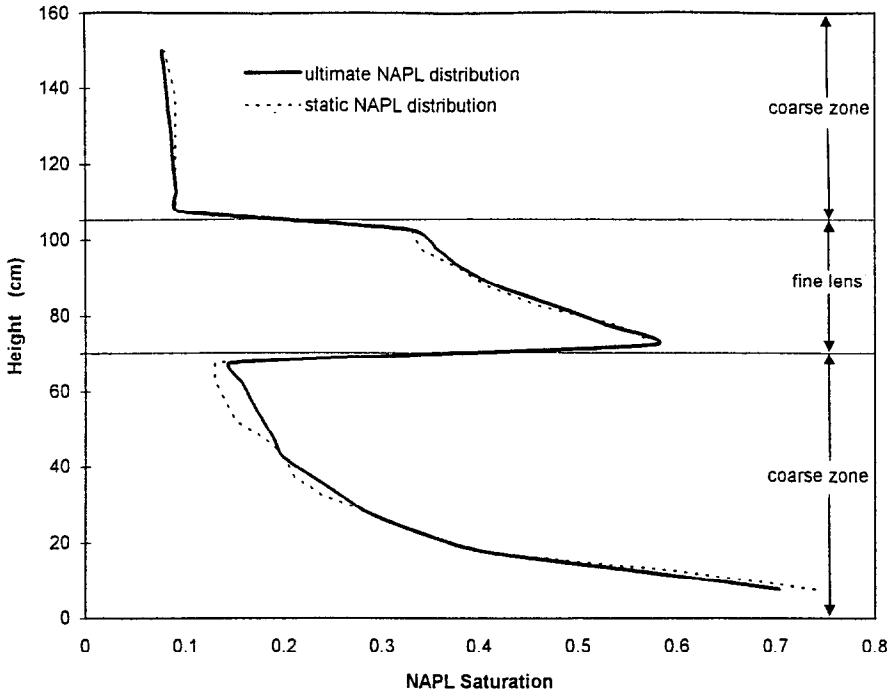

Fig. 2. Static and model predicted ultimate NAPL distribution after infiltration.

The large residual NAPL saturations and the lower permeabilities within the lenses suggested that these zones can ultimately limit the effectiveness of SVE. The volatile components of the oily phase in the more permeable surrounding media will be rapidly removed leaving the essentially saturated capillary entrapped pools. This is illustrated in Fig. 3. An infiltration experiment resulted in the essentially saturated zone at the base of the lens as described above and a uniform residual saturation elsewhere. After application of a vacuum, the infiltrating liquid was removed from the homogeneous coarse sand leaving volatile contaminants only in the region below the partially screened well and at the base of the essentially saturated lens. It is the removal of the saturated residual in the fine grained lens that is the subject of the subsequent soil vacuum extraction experiments and modeling.

3.2. Contaminant removal from a lens by SVE

3.2.1. Pure toluene

In these experiments, pure toluene was injected into the fine lens to simulate the saturated residual that remains after vacuum extraction of the surrounding homogeneous region. The effluent toluene vapor concentration during vacuum extraction is shown in Fig. 4. The model predictions will be described later. The interstitial air velocity above the lens was held constant at $0.73\,cm\,s^{-1}$ during the first stage of the experiment and then increased to $4.7\,cm\,s^{-1}$ after 195 mins.

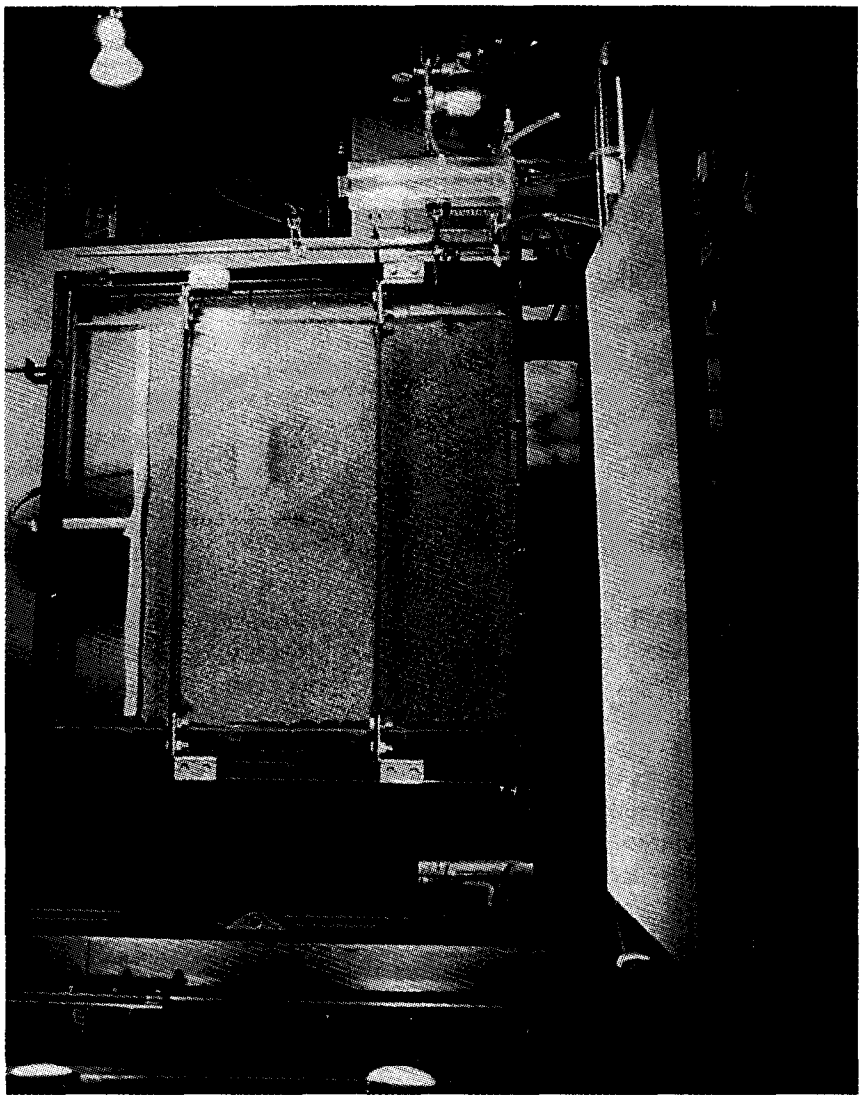

Fig. 3. Ultimate NAPL distribution after infiltration and SVE. Note that high residual remaining at the base of the fine-grained lens to the right of the vacuum well.

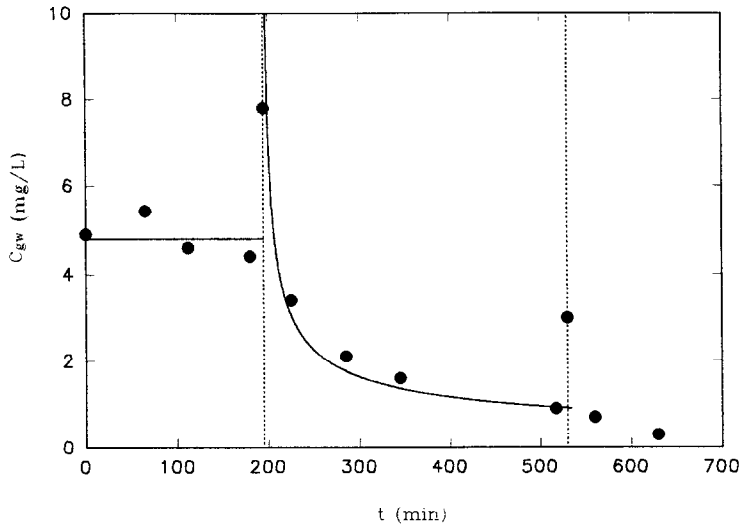

Fig. 4. Measured effluent vapor concentration (C_{gw}: filled circles) and predicted concentration (solid line) in the pure toluene SVE experiment.

The effluent vapor concentration at the extraction well, C_{gw}, (mass of toluene per volume of the vapor at the atmospheric pressure), remained relatively constant at about 4.5 to 5.0 mg L^{-1} in the first stage. This suggested that the rate of mass transfer was controlled by vapor-phase resistances above the lens and that the depletion of toluene within the lens did not appreciably influence the evaporation rate. In the higher air velocity during the second stage, the effluent toluene vapor concentration at the extraction well was relatively large initially, and then decreased rapidly. The initial high concentration may have indicated a rapid increase in flux caused by the elimination of vapor-phase resistances. Continued rapid withdrawal of toluene, however, likely resulted in zone at the surface of the lens depleted of toluene. The slow rate of pore diffusion in the lengthening "dried" zone was likely to be the cause of the rapid decrease in flux transfer with time in the second stage.

After the concentration had decreased to very low levels, the SVE system was shut down for 10 h. Upon renewed application of the vacuum, a classic rebound effect was noted with an initially much higher effluent concentration being observed. This rebound behavior is commonly observed in the field. During the shutdown period, toluene presumably diffused to the edge of the lens and beyond eliminating the intra-lens diffusion resistance and resulting in the elevated effluent concentration after restarting. The excess vapor was rapidly removed from the system and the NAPL effluent concentration returned to that observed prior to the shut-down.

3.2.2. Oily phase mixture

The oily phase mixture experiments were conducted in an identical fashion to the pure phase experiments. A 5% mixture of toluene in automatic transmission oil was injected into the lens at the start of the experiment. The effluent toluene vapor

concentration versus time in the experiment with the oily phase mixture is shown in Fig. 5. Also shown are model predictions to be described later. The initially high concentration is inconsistent with the subsequent slow decrease and may have been affected by the inability to adequately control initial conditions in the experiment. Unlike the previous experiment, sufficient toluene - ATF mixture was injected to fill the entire lens. Any leakage of liquid or vapor from the lens would increase the initial mass transfer area and rate. The slow decrease suggested that the dominant resistances limiting the mass transfer rate out of the lens were those associated with liquid-phase diffusion in the oily phase mixture. A slow decrease of the vapor concentration was also observed in the second stage after increasing the air flow but the liquid phase resistance would be expected to be even more dominant under the higher air flowrate condition. The SVE experiment was again shutdown for 10 h after 440 mins of operation and the rebound effect was observed after reapplying the vacuum.

3.3. Modeling mass transfer rates

3.3.1. Pure toluene — Vapor phase resistances controlling

The essentially constant vapor-phase concentration measured at the extraction well during the first stage of the pure toluene experiment suggested that the removal was controlled by the vapor-phase resistances in the slow moving extractive phase. A conceptual model of toluene mass transfer under these conditions is shown in Fig. 6 (a). It was assumed that toluene resided on the top portion of the lens since the bottom of the lens was initially saturated with water which was not replaced during the filling. The remainder of the lens was assumed to retain residually saturated water at an average saturation of 25%.

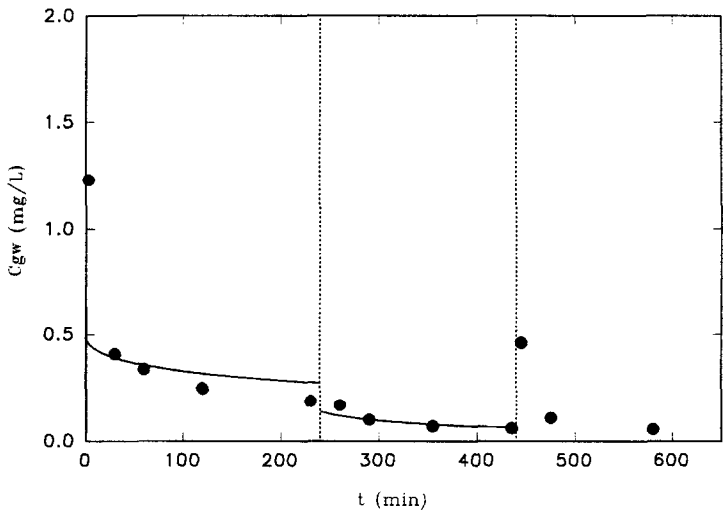

Fig. 5. Measured effluent vapor concentration and predicted concentration in the oily mixture SVE experiment. Mass transfer resistances in both vapor and liquid phases are included in the predictions. Symbol and line are the same in Fig. 4.

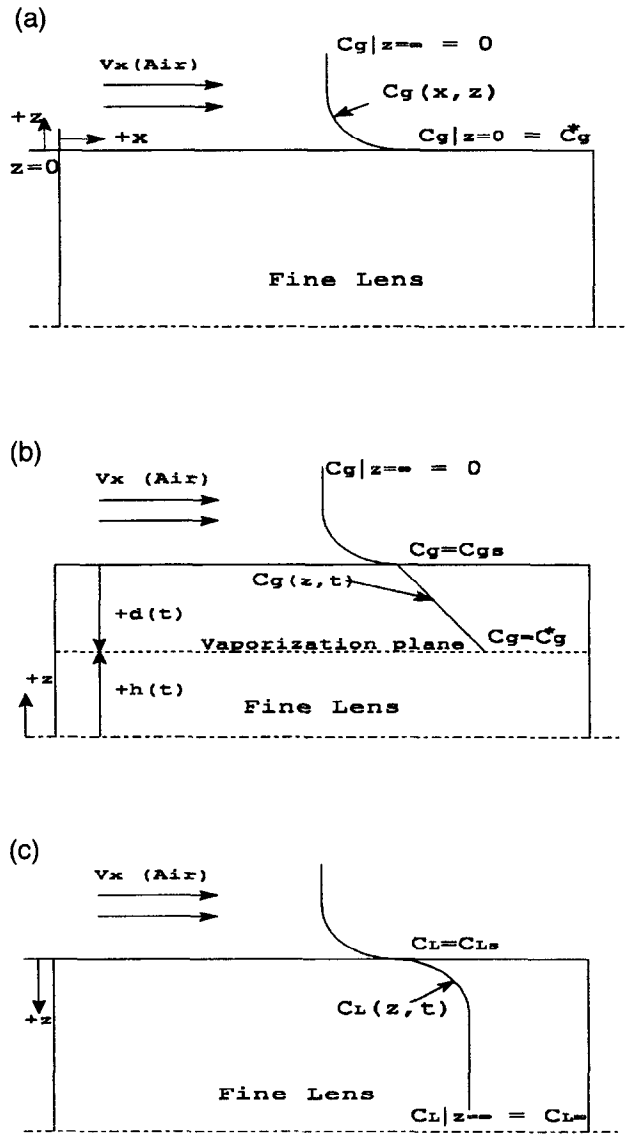

Fig. 6. Schematics of mathematical models for NAPL mass transfer from the lens.

The steady state mass conservation equation of vapor-phase toluene considering only horizontal advection and vertical dispersion from the lens is

$$\epsilon_g V_x \frac{\partial C_g}{\partial x} = K_z \frac{\partial^2 C_g}{\partial z^2} \tag{1}$$

where C_g is the vapor-phase toluene concentration, V_x is an interstitial vapor-phase velocity, ϵ_g is the vapor or gas-filled porosity in the vadose zone, and K_z is an overall

effective dispersion coefficient. z is the distance into the moving vapor stream above the surface of the lens, and x is the distance along the lens from its leading edge. Boundary conditions (BC) for this system assuming the lens surface is $z = 0$ are:

BC 1: $C_g = C_g^*$, at $z = 0 (x, t > 0)$

BC 2: $C_g = 0$, as z goes to infinity $(x, t > 0)$

BC 3: $C_g = 0$, at $x = 0 (z, t > 0)$

BC 1 states that the vapor-phase toluene concentration at the lens surface is in equilibrium with the NAPL phase, i.e., the vapor concentration is given by the pure component vapor pressure of toluene (P_v^*), $C_g^* = P_v^*/(RT)$, where R is the universal gas constant and T is the absolute temperature. BC 2 implies that the toluene concentration well away from the lens surface is zero. BC 3 indicates that there is no vapor-phase toluene at the leading edge of the lens. Johnson et al. [13,14] developed a similar model with different geometry and boundary conditions. The solution to Eq. (1) for the conditions considered here is

$$C_g(x,z) = C_g^* \operatorname{erfc}\left(\frac{z}{2\sqrt{\frac{xK_z}{\epsilon_g V_x}}}\right) \tag{2}$$

and the average toluene flux out of a lens of length L is

$$\text{Flux} = \frac{1}{L}\int_0^L \left(-K_z \frac{\partial C_g(x,z)}{\partial z}\Big|_{z=0}\right) dz = 2C_g^* \sqrt{\frac{K_z V_x \epsilon_g}{\pi L}} \tag{3}$$

Because the evaporation rate of toluene at the lens is equal to its rate of removal at the fully-penetrating extraction well of height, H_w, the average effluent concentration (C_{gw}) is given by

$$C_{gw} = \frac{2C_g^*}{H_w}\sqrt{\frac{K_z L}{\pi \epsilon_g V_x}} \tag{4}$$

and the flux can also be expressed by Flux $= k_g\ C_g^*$ where k_g is a vapor-phase mass transfer coefficient given by

$$k_g = 2\sqrt{\frac{K_z V_x \epsilon_g}{\pi L}} \tag{5}$$

The overall effective dispersion coefficient, K_z, represents the combined effects of molecular diffusion in the soil vapor space and mechanical dispersion induced by air flows above the lens surface [2]. Estimation of dispersion coefficients are problematic in the field but are generally assumed to be of the form,

$$K_z = D_g + \alpha_z V_x \epsilon_g \tag{6}$$

where D_g is the effective molecular diffusion coefficient in the soil vapor space, α_z is

the transverse dispersivity which scales with the size of heterogeneities in the medium. The effective molecular diffusion coefficient can be estimated via the Millington and Quirk model [18] where the effective diffusivity is related to the air or gas-filled porosity (ϵ_g) and total porosity (ϵ) by:

$$D_g = D_a \frac{\epsilon_g^{10/3}}{\epsilon^2} \tag{7}$$

and D_a represents the molecular diffusivity of the evaporating compound in air. The predictive value of Eq. (7) is limited by its sensitivity to moisture content.

The dispersivity under the experimental conditions can be crudely approximated by assuming that the sand pack is equivalent to a bed of uniform diameter spheres. In such a bead pack, the longitudinal dispersivity, α_x, is generally observed to be equal to one-half of the bead diameter while the transverse dispersivity, α_z, is normally assumed to be 5–10 times smaller. Using the mean particle diameter of the sand, the estimated velocity, and transverse dispersivity 10 times smaller than the longitudinal, the estimated dispersion coefficient, K_z, was 0.015 cm^2 s^{-1} and a corresponding value of k_g predicted by Eq. (5) was 0.0173 $cm\,s^{-1}$. All model parameters are summarized in Table 3. The effluent concentrations predicted by this approach (4.8 $mg\,L^{-1}$) were in good agreement with the observations. The experimentally observed value of k_g was about 0.0181 $cm\,s^{-1}$.

3.3.2. *Pure toluene — Intra-lens resistances controlling*

To describe toluene mass transfer under high flowrate conditions, a "receding front" model was employed. This model, which is similar to that employed by Thibodeaux [19] and Thibodeaux and Hwang [20], assumes that as the toluene evaporated, a "dried-out" zone developed near the lens surface. As further vaporization occurs, the thickness of this dried zone increases. Due to the relatively low permeability of the fine-grained lens, it was assumed that there was no significant advection in the dried zone, and that movement into the extracting vapor-phase was the result of quasi-steady diffusion through the dried zone to the surface of the lens. The effective diffusion coefficient was again estimated by the Millington and Quirk model, and the water content in the lens was assumed to remain constant at residual water saturation levels.

The conceptional schematic of the "receding front model" is shown in Fig. 6 (b), where $h(t)$ is the time dependent liquid toluene height, and $d(t)$ is the depth of the dry

Table 3
Experimental parameters used in modeling of the first stage of pure toluene experiment

Parameter	Value
K_z	0.015 $cm^2\,sec^{-1}$
C_g^*	143 $mg\,L^{-1}$
H_w	33 cm
L	14 cm
V_x	0.73 $cm\,sec^{-1}$
ϵ_g	0.3

zone. $d(t)$ increases with time while $h(t)$ decreases according to a mass balance on the amount of toluene lost. In this model, the vapor-phase toluene concentration at the vaporization plane was assumed to be equivalent to the toluene vapor pressure, C_g^*. Resistances external to the lens were included in the model for completeness, but were apparently quite small at the higher flowrate. The vapor concentration at the lens surface (C_{gs}) can be obtained from the quasi-steady state assumption and the mass balance between the rate of diffusion through the dried zone and the rate of mass transfer out of the lens,

$$-D_g \frac{C_g^* - C_{gs}}{d(t)} = k_g C_{gs} \tag{8}$$

C_{gs} is given by

$$C_{gs} = \frac{C_g^*}{1 + \dfrac{d(t)k_g}{D_g}} \tag{9}$$

A mass balance between the rate of change of liquid toluene and rate of toluene loss from the lens surface gives the depth of the liquid pool of toluene in the lens.

$$d(t) = D_g \left[\sqrt{\frac{1}{k_g^2} + \frac{2C_g^* t}{\rho_o \epsilon S_o D_g}} - \frac{1}{k_g} \right] \tag{10}$$

where ρ_o is the mass density of the liquid toluene (or other oily phase), ϵ is the total porosity of the lens, and S_o is the residual oily phase (liquid toluene) saturation within the top region of the lens (assumed constant and equal to 75% in the current experiment, i.e., liquid toluene fills the entire pore space remaining after retention of residual water). Note that Eq. (10) indicates that if the mass transfer resistances external to the lens control the evaporation, the depth of the "dried-out" zone is effectively constant and negligible. For large k_g, however, the zone depleted of toluene increases with the square root of time and the rate of mass transfer decreases at a rate inversely proportional to the size of this zone.

The average vapor concentration at the extraction well was obtained from an overall mass balance,

$$C_{gw}(t) = \frac{D_g L}{V_x \epsilon_g H_w} \frac{(C_g^* - C_{gs})}{d(t)} \tag{11}$$

The parameters used in this model are summarized in Table 4.

The predicted concentrations without mass transfer resistances external to the lens are compared with measurements in the middle portion of Fig. 4 and in Fig. 7. The effects of the external mass transfer resistances on predicted effluent concentrations are also shown in Fig. 7. The "receding front" model without external mass transfer resistances accurately predicted the observed behavior. For the purposes of this calculation, any small depletion caused by the initial low air flow during the first stage of the experiment was neglected. When transport is controlled by the external resistances, redistribution of the toluene within the lens is comparatively rapid.

Table 4
Experimental parameters used in modeling of second stage of pure toluene experiment

Parameter	Value
D_g	$0.0099\,cm^2\,s^{-1}$
C_g^*	$1.43\times10^{-4}\,g\,cm^{-3}$
k_g	$0.108\,cm\,s^{-1}$
ρ_o	$0.866\,g\,cm^{-3}$
ϵ	0.4
S_o	0.75
V_x	$4.7\,cm\,s^{-1}$
ϵ_g	0.3
L	14 cm
H_w	33 cm

3.4. Oily mixture — Vapor and liquid phase resistances controlling

If the toluene is present in a mixture, intra-lens diffusion, i.e., liquid-side mass transfer resistances, may arise. A model allowing for both vapor and liquid phase resistances was developed to describe the two stages of the experiment. Because the oily mixture was 95% nonvolatile ATF, any liquid recession was neglected.

The concept of the model is shown in Fig. 6 (c). It is assumed in the model that the change in vapor-phase concentration along the top surface of the lens was negligible. The governing equation of the transport of toluene in the oily mixture lens is then:

$$\frac{\partial(\epsilon S_o C_L)}{\partial t} = D_L \frac{\partial^2 C_L}{\partial z^2} \tag{12}$$

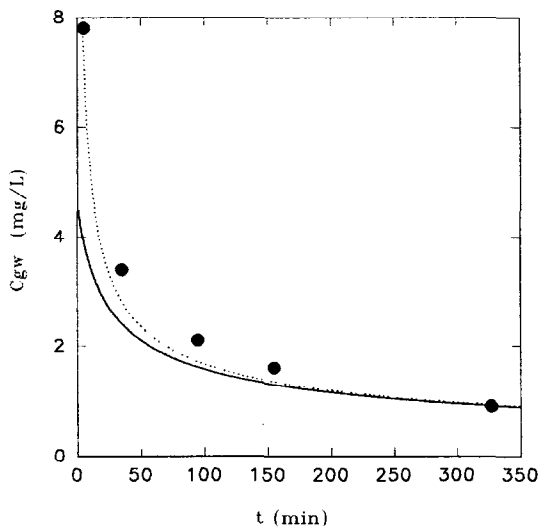

Fig. 7. Comparison of predicted concentrations with and without vapor phase resistances with measurements in the pure toluene SVE experiment.

and the initial condition (IC) and boundary conditions are,

IC: $C_L = C_{L\infty}$ at t = 0
BC 1: $C_L = C_{L\infty}$ as z goes to infinity
BC 2: $D_L \frac{\partial C_L}{\partial z} = k_g^* C_{Ls}$ at the interface of the lens ($z = 0$)

where C_L is the liquid toluene concentration in the oily phase. The initial liquid toluene concentration, $C_{L\infty}$, is assumed to be uniform throughout the lens. The oily phase is again assumed to fill all available pore space not occupied by residual water (i.e., $S_o \sim 0.75$, $\epsilon_o = 0.3$). D_L is the effective molecular diffusion coefficient of toluene within the oily liquid mixture, and k_g^* is the vapor-phase mass transfer coefficient of the mixture based on the liquid-phase concentration. The solution to Eq. (12) is given by Slattery [21]:

$$\frac{C_L}{C_{L\infty}} = \operatorname{erf}\left(\frac{z}{\sqrt{4D_L t/\epsilon_o}}\right) + \exp\left(\frac{k_g^* z}{D_L} + \frac{k_g^{*2} t}{D_L \epsilon_o}\right) \times \operatorname{erfc}\left(\frac{z}{\sqrt{4D_L t/\epsilon_o}} + \frac{k_g^*}{D_L}\sqrt{D_L t/\epsilon_o}\right) \quad (13)$$

The average vapor-phase toluene concentration at the well is then calculated from the overall mass balance.

$$C_{gw}(t) = \frac{2C_{L\infty} k_g^* L}{\epsilon_g V_x H_w} \exp\left(\frac{k_g^{*2} t}{D_L \epsilon_o}\right) \operatorname{erfc}\left(\frac{k_g^*}{D_L}\sqrt{\frac{D_L t}{\epsilon_o}}\right) \quad (14)$$

If the vapor-phase resistances are negligible as expected at the higher flowrate in the second stage, the toluene concentration at the lens surface is assumed to be zero. The governing equation for this case is exactly the same as the previous case but BC 2

Table 5
Experimental parameters used in modeling of oily mixture experiment

Parameter	Value
D_L	1.13×10^{-6} cm^2 s^{-1}
$C_{L\infty}$	0.043 g cm^{-3}
k_g^*	3.06×10^{-6} +, 1.83×10^{-5} cm s^{-1}
V_x	0.73 +, 4.4 cm s^{-1}
H_w	34 cm
L	14 cm
ϵ_g	0.3
ϵ_o	0.3

+ 1st stage of oily mixture experiment.

changes to $C_L = 0$ at $z = 0$ for $t > 0$. The average concentration at the extraction well then becomes

$$C_{gw}(t) = \frac{2C_{L\infty}}{\epsilon_g V_x}\left(\frac{L}{H_w}\right)\sqrt{\frac{D_L \epsilon_o}{\pi t}} \tag{15}$$

The parameter values for this experiment are listed in Table 5. The experimental data collected during the first (lower flowrate) and second (higher flowrate) stages were compared to those predicted by Eq. (14) and Eq. (15), respectively. Since both internal and external resistances are important, it is not possible to neglect initial depletion within the lens during the first stage of the experiment as was assumed in the pure toluene experiment. The effect of the initial depletion on the effluent concentrations in the second stage was approximated by shifting time in Eq. (14) for the second stage: the time shift was estimated by the time required to extract the mass depleted during the first stage under the second stage conditions and was 40 mins. The "start" of sampling during the second stage was thus expected to be equivalent to $t = 40$ mins in Eq. (14).

The effects of the external mass transfer resistances on the extraction well concentrations are also illustrated in Fig. 8 and Fig. 9 for each stage. The vapor-phase resistances were significant in the lower flowrate stage of the experiment but were negligible in the higher flowrate stage when liquid-phase resistances controlled the overall mass transfer. The models accurately predicted the magnitude of the toluene concentration at the extraction well in both stages.

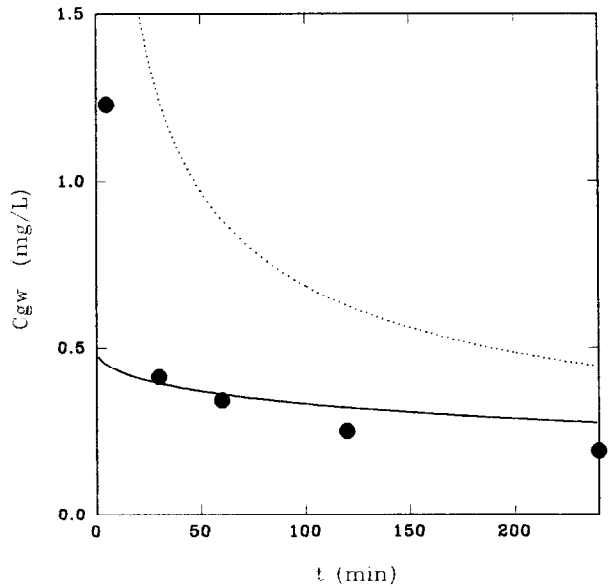

Fig. 8. Comparison of predicted concentrations with and without vapor phase resistances with measurements in the first stage of the oily mixture SVE experiment.

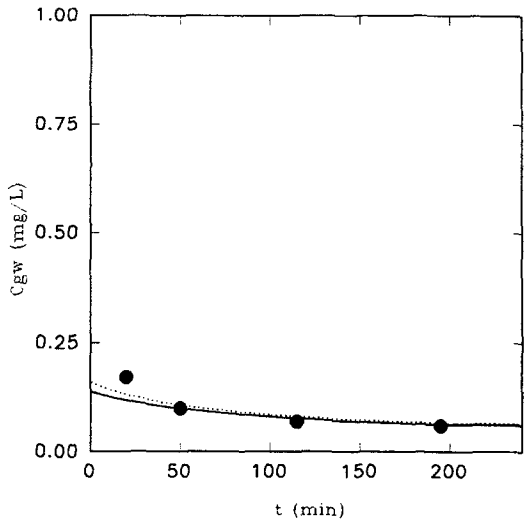

Fig. 9. Comparison of predicted concentrations with and without vapor phase resistances with measurements in the second stage of the oily mixture SVE experiment.

The initial dynamics during the low flowrate stage, however, were not well predicted. This may have reflected inadequacies of the model, in particular, the inappropriateness of the simple initial conditions used in the model or artifacts resulting from the leakage during the injection of the oily mixture in the fine lens. The slow mass transfer rate after the initial concentration measurement was not consistent with the rapid rate reflected by the initial measurement, suggesting experimental artifact.

4. Conclusions

Laboratory infiltration experiments with an oily phase in a heterogeneous unsaturated zone suggested that significant quantities of the NAPL may be entrapped within and not pooled at the surface of low-permeability lenses. The entrapped NAPL, resulting from capillary forces, would be expected to pose the greatest resistance to soil remediation by soil vacuum extraction.

Soil vacuum extraction experiments on a pure residual NAPL phase in such a lens indicated that it was possible to model the release based on air-side mass transfer resistances at low air flowrates ($Re \leq 0.5$) and by considering vapor diffusion in the drying portion of the lens at higher air flows ($Re \geq 3$). Similar experiments with an oily phase mixture indicated that it was also possible to predict the release of the volatile constituent by consideration of both air and liquid side mass transfer resistances at low air flowrates. At high air flowrates, the evaporation of the volatile constituent was controlled mainly by liquid-side mass transfer resistances.

The experiments provided validation of relatively simple modeling approaches for predicting soil vacuum extraction rates from entrapped pure and mixture NAPLs in low permeability media under low, as well as high air flow conditions.

Acknowledgements

The authors would like to acknowledge the support of the US Environmental Protection Agency and LSU Hazardous Waste Research Center, Cooperative Agreement no. CR-813888-01 and the National Science Foundation and the Louisiana Educational Quality Support Funt, Grant # NSF/LaSER-ADP-03.

References

[1] D.J. Wilson and A.N. Clarke, in Hazardous Waste Site Soil Remediation: Theory and Application of Innovative Technologies, Marcel Dekker, Inc., New York, 1994.
[2] J.L. Smith, in An Experimental Study of the Transport and Fate of a NAPL in a Heterogeneous Soil and Its Removal by Vacuum Extraction, MS Thesis, Louisiana State University, Baton Rouge, LA, 1994.
[3] C.P. Ardito and J.F. Billing, in Alternative remediation strategies: The subsurface volatilization and ventilation system, Proceedings of the NWWA/API Conference on Petroleum Hydrocarbons and Organic Chemicals in Groundwater: Prevention, Detection and Restoration, Houston, Texas, 1990, pp. 281–296.
[4] S.B. Blake and M.M. Gate, in Vacuum enhanced hydrocarbon recovery: A case study: Proceedings of the NWWA/API Conference on Petroleum Hydrocarbons and Organic Chemicals in Groundwater: Prevention, Detection and Restoration, Houston, Texas, 1986, pp. 709–721.
[5] W.L. Crow, E.P. Anderson and E.M. Minugh, Ground Water Monit. Rev., 7 (1987) 51.
[6] N.J. Hutzler, B.E. Murphy and J.S. Gierke, in State of Technology Review: Soil Vapor Extraction Systems, Cooperative Agreement CR-814319-01-1, Hazardous Water Research Laboratory, EPA, Cincinnati, OH, August, 1988.
[7] A.N. Clarke, R.D. Mutch, P.D. Mutch and D.J. Wilson, in In situ vapor stripping: Results of a year-long pilot study, Eckenfelder, Inc., Mahwah, N.J., 1990.
[8] J.S. Thornton and W.L. Wootan, Environ. Progress, 1 (1982) 42.
[9] Texas Research Institute: Forced venting to remove gasoline vapors from a large scale model aquifer, API publication no. 4431, 1984.
[10] G.E. Hoag, M.C. Marley, J. Environ. Eng., 112 (1984) 586.
[11] S. Lingineni and U.K. Dhir, in Modeling of soil venting systems to remediate unsaturated soils, ASCE Specialty Conference, July 8–11, Arling, VA, USA, 1990.
[12] H.W. Parker, K.A. Rainwater, B.J. Claborn and M.R. Zaman, in Diffusion control model for vaporization of hydrocarbon contamination from the vadose zone, Spring National Meeting of Amer. Inst. of Chem. Eng., Houston, TX, 1989.
[13] P.C. Johnson, M.W. Kemblowski and J.D.Colthart, in Practical screening models for soil venting applications, Proc. of the NWWA/API Conference on Petroleum Hydrocarbons and Organic Chemicals in Groundwater, Houston, TX, 1988.
[14] P.C. Johnson, M.W. Kemblowski and J.D. Colthart, Groundwater, 28 (1990) 413.
[15] Computer Modelling Group (CMG), Imex 300-DX User's Manual, 1992.
[16] H.C. Slider, in Practical Petroleum Reservoir Engineering Methods, Petroleum Publishing Company, 1976.
[17] M. Honarpour, L. Koedertz and A.H. Harvey, Relative Permeability of Petroluem Reservoirs, CRC Press, 1986.
[18] R.J. Millington and J.P. Quirk, Trans. Faraday Soc., 57 (1961) 1200.
[19] L.J. Thibodeaux, in Chemodynamics: Environmental Movement of Chemicals in Air, Water, and Soil, John Wiley and Sons, NY, 1979.
[20] L.J. Thibodeaux and S.T. Hwang, Environmental Progress, 1 (1982) 42.
[21] J.C. Slattery, in Momentum, energy, and mass transfer in continua, McGraw-Hill, Inc., 1972.